Title
Preservation of a remote fear memory requires new myelin formation

Author
Pan, Simon

Publication Date
2020

Peer reviewed|Thesis/dissertation

Preservation of a remote fear memory requires new myelin formation

by
Simon Pan

DISSERTATION
Submitted in partial satisfaction of the requirements for degree of
DOCTOR OF PHILOSOPHY

in

Neuroscience

in the

GRADUATE DIVISION
of the
UNIVERSITY OF CALIFORNIA, SAN FRANCISCO

Approved:

DocuSigned by:
Jonah Chan
C3B6323AB15D485...

Jonah Chan
Chair

DocuSigned by:
Mazen Kheirbek
DocuSigned by:
Vikaas Sohal
DocuSigned by:
Samuel Pleasure
05586C7D64D24A2...

Mazen Kheirbek
Vikaas Sohal
Samuel Pleasure

Committee Members

Dedication and Acknowledgments

I would like to thank my advisors, Drs. Jonah R. Chan and Mazen A. Kheirbek for their support in conducting my dissertation research.

I would like to thank the UCSF MSTP program for providing me with an opportunity to pursue the dual doctorate degree.

Most of all, I would like to thank my parents for raising me and providing me with the financial support to complete these academic pursuits.

Contributions

The scientific work described in this dissertation is currently in press at *Nature Neuroscience*.

Pan, S., Mayoral, S.R., Choi H.S., Chan, J.R., Kheirbek, M.A. Preservation of a remote fear memory requires new myelin formation. Nat Neurosci (2020) **doi:** 10.1038/s41593-019-0582-1

Preservation of a remote fear memory requires new myelin formation

Simon Pan

Abstract

Experience-dependent myelination is hypothesized to shape neural circuit function and subsequent behavioral output. Using a contextual fear memory task in mice, we demonstrate that fear learning induces oligodendrocyte precursor cells (OPCs) to proliferate and differentiate into myelinating oligodendrocytes (OLs) in the medial prefrontal cortex (mPFC). Transgenic animals which cannot form new myelin exhibit deficient remote, but not recent, fear memory recall. Recording population calcium dynamics with fiber photometry, we observe that the neuronal response to conditioned context cues evolves over time in the mPFC, but not in animals that cannot form new myelin. Finally, we demonstrate that pharmacological induction of new myelin formation with clemastine fumarate improves remote memory recall and promotes fear generalization. Thus, bidirectional manipulation of myelin plasticity functionally impacts behavior and neurophysiology, suggesting that neural activity during fear learning instructs the formation of new myelin, which, in turn, supports the consolidation and/or retrieval of remote fear memories.

Table of Contents

List of Figures

Chapter 1: Introduction

The formation of enduring memories requires anatomical substrates that are both plastic, to represent new experiences, as well as perseverant, to preserve lasting representations of those experiences. Although the majority of myelination occurs during postnatal development, oligodendrocyte precursor cells (OPCs) persist in the adult brain and continually proliferate and differentiate to produce myelinating oligodendrocytes (OLs) throughout life[1,2,3,4,5,6]. OPCs exhibit excitatory postsynaptic potentials in response to neurotransmitter release[7,8] and, in adult rodents, optogenetic or chemogenetic stimulation of neurons is sufficient to induce proliferation, differentiation, and maturation of cortical OPCs into myelinating OLs[9,10,11]. Naturalistic experiences such as motor learning, social isolation, environmental enrichment, and sensory deprivation are similarly able to regulate OPC proliferation and differentiation, raising the possibility that experience-induced myelin formation may represent an alternative, or additional, modality of structural remodeling during learning, distinct from synaptic plasticity[12,4,13,14,15,16,17]. Notably, studies monitoring the dynamics of OL populations over time through pulse-chase labeling or longitudinal *in vivo* two photon imaging report that myelinating OLs are extraordinarily stable upon formation, uniquely positioning new myelin formation as a durable substrate to support lifelong memories[1,3,18].

Myelination confers profound changes in the biophysical and molecular properties of axons, increasing transmembrane resistance, decreasing membrane capacitance, and coordinating architectural rearrangements of voltage-gated ion channels to enable rapid saltatory conduction[19]. Although it is well appreciated that myelination increases conduction velocity across individual axons, how this translates to computations at the level of neural circuits and their subsequent behavioral outputs is poorly understood[20]. Inhibition of new myelin formation prior to presenting adult mice to a complex wheel with missing rungs impairs motor learning,

demonstrating that new myelin formation is important for skilled learning[15,17]. However, it is not known what abnormalities in circuit activity underlie these behavioral deficits, nor whether these findings extend to other learning modalities, such as episodic and emotional memory, which are very distinct in their anatomical basis, mnemonic content, and clinical significance.

Fear memory is a highly evolutionarily conserved behavior critical for evaluating and responding to threatening situations and can become pathologically maladaptive in neuropsychiatric diseases such as post-traumatic stress disorder (PTSD)[21,22]. Over time, fear memories become consolidated via a process involving reorganization of neuronal networks into a stable memory trace that can be recalled at least several weeks later, referred to as remote memory. While a number of studies have identified putative circuits that are involved in the consolidation of remote memories[23,24,25,26,27]. the cellular and synaptic mechanisms through which remote memories are consolidated, maintained, and retrieved remain an active area of investigation[28,29]. We found that contextual fear conditioning induced OPCs to proliferate and mature into myelinating OLs in the medial prefrontal cortex (mPFC). To examine the functional significance of this new myelin formation in fear learning, we assessed fear memory in transgenic mice that are unable to form new oligodendrocytes and found that remote fear memory recall was impaired in the absence of oligodendrogenesis. Furthermore, increasing new myelin formation through administration of the pro-myelinating compound clemastine fumarate preserved retrieval of remote fear memory. In both cases, immediate early gene expression in fear-associated brain regions paralleled the changes in learning performance. To probe this neurophysiological deficit with greater temporal resolution, we recorded population calcium dynamics in freely behaving mice via fiber photometry and observed altered prefrontal activity in the absence of new oligodendrogenesis during remote, but not recent, memory recall. Collectively, these findings suggest a reciprocal relationship in which learning experience induces new myelin formation that, in turn, supports the neural circuits of remote fear memories.

Chapter 2: Fear learning experience induces new myelin formation

Fear learning experience induces OPC proliferation in the medial prefrontal cortex.

To determine if fear learning induces OPC proliferation and differentiation, we injected wildtype 8-week old male C57BL/6J mice with of 5-ethynyl-2'-deoxyuridine *(*EdU), a thymidine analogue that is incorporated by actively proliferating cells, and immediately subjected them to contextual fear conditioning (Figure 2.1a). 24 hours post-conditioning, conditioned mice froze in the conditioning context, indicative of successful learning of the shock-context association (Figure 2.1b), and were then perfused for subsequent histological analysis. We detected an increase in the number of total EdU^+ cells and $EdU^+/Olig2^+$ OPCs in the mPFC of conditioned mice compared to home cage controls (Figure 2.1c-f). As novel context exposure and the foot shock stress can conceivably induce these changes, we included two additional control groups in which the mice either received a context-only exposure (no shock; NS) or were shocked immediately upon being put in the chamber and promptly removed (immediate shock; IS). Both groups of mice displayed low levels of freezing during the retrieval session (Figure 2.1b), indicating the absence of learning, and correspondingly showed no changes in the number of $EdU^+/Olig2^+$ cells (Figure 2.1c-d). These results indicate that fear learning experience, independently of novel context exposure or foot shock stress, induces a rapid increase in OPC proliferation in the mPFC.

Fear learning experience induces OPC maturation into myelinating OLs in the medial prefrontal cortex.

Next, we determined if this brisk proliferation of OPCs culminated in their maturation to myelinating OLs. We conducted an extended experiment in which the mice were injected with EdU for five consecutive days and then fear conditioned, with their freezing responses

measured during retrieval sessions occurring 24 hours and 30 days post-conditioning (Figure 2.2a). Freezing responses were maintained over the course of the experiment (Figure 2.2a) and the number of EdU^+ cells co-localizing with ASPA, a marker for differentiated OLs, was increased in the mPFC with no change in the total amount of $EdU^+/Olig2^+$ cells (Figure 2.2c-e). Finally, we performed electron microscopy 30 days post-conditioning and found that fear learning experience significantly increased the density of myelinated axons in the mPFC of fear-conditioned animals compared to home cage controls (Figure 2.2f-h).

OPC maturation into myelinating OLs occurs over several weeks in adult gray matter.

To examine the timing of OL maturation in adult gray matter, we quantified the density of $EdU^+/ASPA^+$ cells and GFP^+/MBP^+ (myelin basic protein) cells in the mPFC, BLA, and dHPC of *tau-mGFP*$^{loxP/loxP}$*;NG2CreERT*$^+$ mice that were injected with EdU for five consecutive days, fear conditioned, and then perfused after their 7, 14, or 30 day retrieval sessions (Figure 2.3a). In this line, membrane-bound GFP adjacent to a floxed stop codon is expressed under the *tau* promoter. *NG2CreERT* is an inducible cre line specific to OPCs, while the *tau* promoter is active in OLs but not OPCs. Thus, recombined OPCs that successfully differentiate into Ols are exclusively visualized by the expression of GFP. We can further distinguish mature, myelinating Ols from immature, non-myelinating Ols through the presence of distinctive myelin internodes that co-localize with MBP (Figure 2.3b-c). We observed that the density of $EdU^+/ASPA^+$ cells and GFP^+/MBP^+ cells was virtually zero in animals 7 days post-tamoxifen and -EdU but increased significantly at 14 and 30 days, while the density of GFP^+/MBP^- pre-myelinating OLs remained similar across time (Figures 2.3d-e).

Next, we analyzed co-localization of ASPA, GFP, and MBP in *tau-mGFP*$^{loxP/loxP}$*;NG2CreERT*$^+$ animals perfused at 30 days and found that $ASPA^+/GFP^+$ cells were exclusively MBP^+ OLs with myelinating morphology and conversely, that GFP^+/MBP^+ OLs with myelinating morphology

were exclusively ASPA$^+$ (Figures 2.3f-g), demonstrating that ASPA is a specific marker for mature, myelinating OLs. These data suggest that although OPC proliferation and differentiation can occur rapidly, maturation and compact myelin formation in adult gray matter takes place over a prolonged timescale of several weeks. Importantly, the validation of ASPA as a marker of mature, myelinating OLs signifies that the increase in EdU$^+$/ASPA$^+$ cells in the mPFC that we observed in response to fear learning (Figure 2.2c-e) was indicative of new myelin formation.

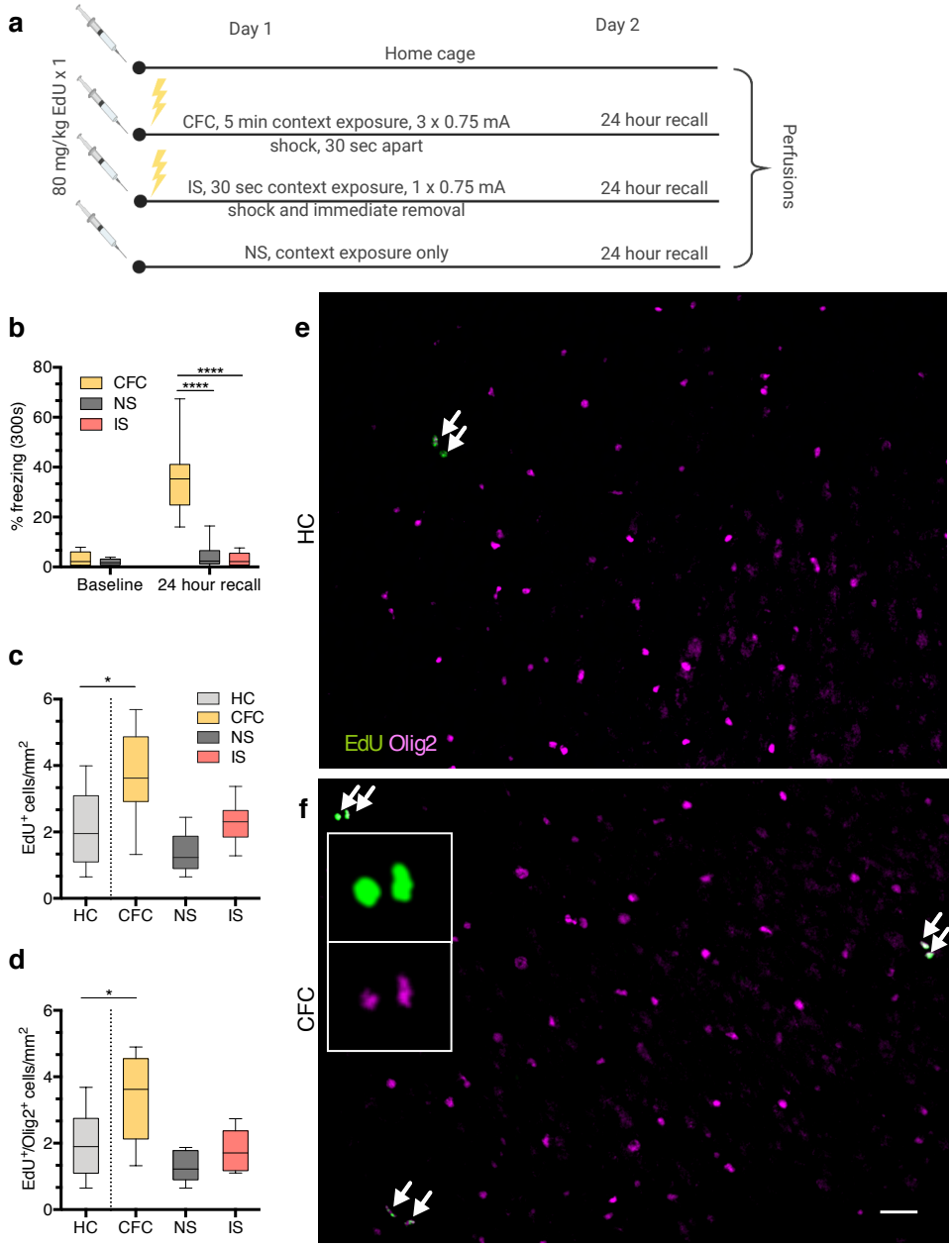

Figure 2.1. Fear learning induces OPC proliferation in the mPFC. (**a**) Experimental paradigm for EdU injections and contextual fear conditioning. (**b**) Freezing responses pre-shock and during 24 hour recall for home cage (HC), fear conditioned (CFC), no shock (NS), and immediate shock (IS) groups; one-way ANOVA ($F_{2,20} = 28.35$, $p < 0.0001$) with Sidak's *post hoc* tests comparing CFC vs. NS (difference: -31.19 ± 6.179, 95% CI: -44.54 to -17.84, $p < 0.0001$) and CFC vs. IS (difference -32.94 ± 5.536, 95% CI: -44.81 to -21.07, $p < 0.0001$). (**c**) Total EdU^+ cell density in the mPFC of HC, CFC, NS, and IS animals; one-way ANOVA ($F_{3,26} = 7.238$, $p = 0.0012$) with Sidak's *post hoc* tests comparing HC vs. CFC (difference: -1.616 ± 0.5212, 95% CI: -2.946 to -0.2868, $p = 0.0137$), HC vs. NS (difference: 0.7080 ± 0.5382, 95% CI: -0.6654 to 2.081, $p = 0.4878$), and HC vs. IS (difference: -0.1819 ± 0.5212, 95% CI: -1.512 to 1.148, $p = 0.9803$). (**d**) $EdU^+/Olig2^+$ cell density in the mPFC of HC, CFC, NS, and IS animals; one-way ANOVA ($F_{3,26} = 7.672$, $p = 0.0008$) with Sidak's *post hoc* tests comparing HC vs. CFC (difference: -1.393 ± 0.47, 95% CI: -2.592 to -0.1933, $p = 0.0192$), HC vs. NS (difference: 0.7474 ± 0.4854, 95% CI: -0.4912 to 1.986, $p = 0.3544$), and HC vs. IS (difference: 0.1734 ± 0.47, 95% CI: -1.026 to 1.373, $p = 0.9769$) at 24 hours post-conditioning. Representative images of EdU (green) and Olig2 (magenta) staining in the mPFC of home cage (**e**) and fear-conditioned (**f**) animals, arrows indicate co-localized $EdU^+/Olig2^+$ cells; inset depicts separate color channels for representative $EdU^+/Olig2^+$ cells (top left). For all panels, n = 7 mice (HC), 8 mice (CFC), 7 mice (NS), 8 mice (IS). Scale bar: 50 μm. For box-and-whisker plots, the center, boxes, and whiskers represent the median, interquartile range, and the 10th and 90th percentiles, with asterisks indicating the following p-value ranges: * ≤ 0.05, **** ≤ 0.0001.

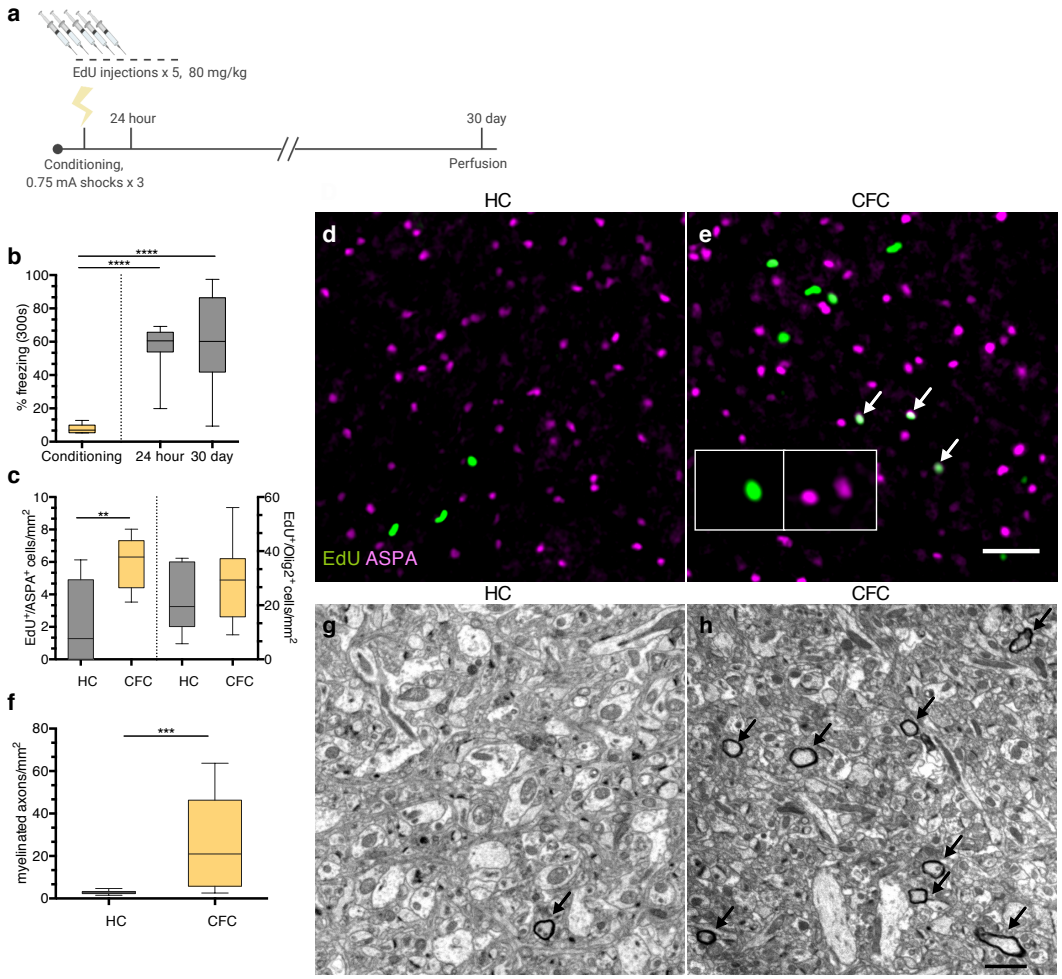

Figure 2.2. Fear learning experience induces OPC maturation into myelinating OLs in the mPFC. (**a**) Experimental paradigm for EdU injections and contextual fear conditioning. (**b**) Freezing responses during pre-conditioning and 24 hour and 30-day retrieval sessions; one-way ANOVA ($F_{2,21}$ = 19.42, p < 0.0001) with Sidak's *post hoc* tests comparing conditioning vs. 24 hour (difference: -48.53 ± 9.402, 95% CI: -71.17 to -25.89, p < 0.0001) and conditioning vs. 30 day (difference: -52.71 ± 9.402, 95% CI: -75.34 to -30.07, p < 0.0001). (**c**) $EdU^+/ASPA^+$ (left bars) and $EdU^+/Olig2^+$ (right bars) density in the mPFC of home cage (HC) and fear conditioned (CFC) animals at 30 days post-conditioning; unpaired two-tailed t-tests for HC vs. CFC for $EdU^+/ASPA^+$ (difference: 3.629 ± 1.125, 95% CI: 1.199 to 6.060, t_{13} = 3.226, p = 0.0066) and $EdU^+/Olig2^+$ (difference: 7.555 ± 6.944, 95% CI: -7.446 to 22.56, t_{13} = 1.088, p = 0.2963) cell density. Representative images of EdU (green) and ASPA (magenta) in the mPFC of home cage (**d**) and fear conditioned (**e**) animals, arrows indicate co-localized $EdU^+/ASPA^+$ cells; inset depicts separate color channels for representative $EdU^+/ASPA^+$ cell (left-most). (**f**) Quantification of myelinated axon density per field of view in the mPFC; unpaired two-tailed t-tests comparing HC vs. CFC (difference: 23.07 ± 5.882, 95% CI: 10.95 to 35.18, t_{25} = 3.922, p = 0.0006). Representative electron micrographs of myelinated axons (arrows) in mPFC gray matter for HC (**g**) and CFC (**h**) animals. (**b-c**) n = 7 mice (HC) and 8 mice (CFC), (**f**) n = 5 mice (HC) and 4 mice (CFC), 3 fields of view per mouse. Scale bar: 50 (**d-e**) μm, (**g-h**) 2 μm. For box-and-whisker plots, the center, boxes, and whiskers represent the median, interquartile range, and the 10^{th} and 90^{th} percentiles, with asterisks indicating the following p-value ranges: ** ≤ 0.01, *** ≤ 0.001, **** ≤ 0.0001.

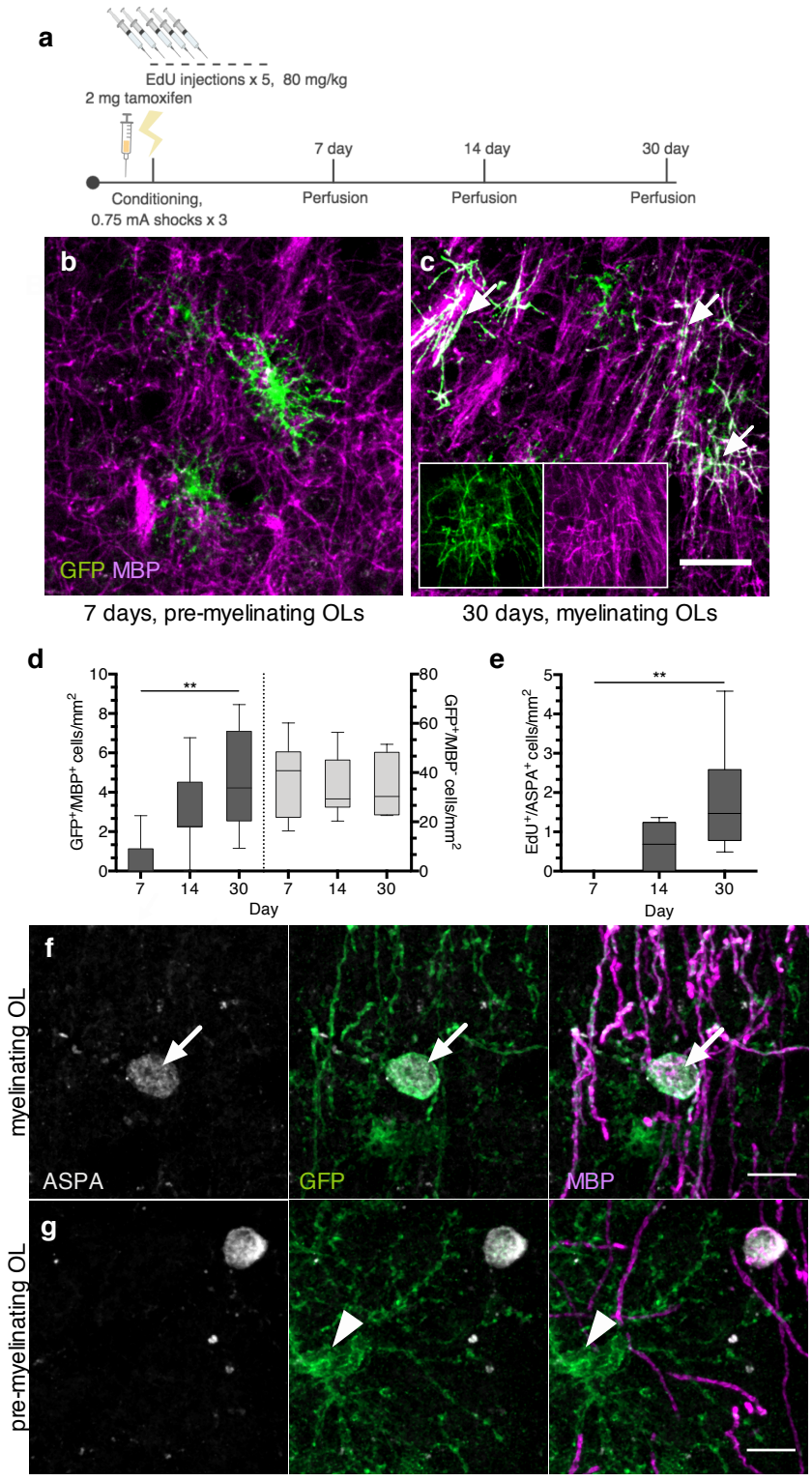

Figure 2.3. OPC maturation into myelinating OLs occurs over several weeks in adult gray matter. (**a**) Experimental paradigm for tamoxifen injections, EdU injections, contextual fear conditioning, and perfusions. Representative images of GFP^+ (green)/MBP^- (magenta) pre-myelinating OLs at 7 days post-tamoxifen (**b**) and GFP^+/MBP^+ myelinating OLs (arrows) at 30

days post-tamoxifen (**c**) in the mPFC of fear conditioned mice; inset depicts separate color channels for representative GFP^+/MBP^+ cell (left-most). (**d**) Quantification of GFP^+/MBP^+ (left bars) and GFP^+/MBP^- (right bars) cell density in the mPFC over time; for GFP^+/MBP^+ density (left bars), one-way ANOVA ($F_{2,19} = 6.586$, $p = 0.0067$) with Sidak's *post hoc* tests comparing 7 vs. 14 days (difference: -2.695 ± 1.070, 95% CI: -5.292 to -0.09785, $p = 0.0614$) and 7 vs. 30 days (difference: -4.045 ± 1.129, 95% CI: -6.787 to -1.304, $p = 0.004$); for GFP^+/MBP^- density (right bars) one-way ANOVA ($F_{2,21} = 0.07572$, $p = 0.9274$) with Sidak's *post hoc* tests comparing 7 vs. 14 days (difference: 2.354 ± 6.908, 95% CI: -14.41 to 19.12, $p = 0.9308$) and 7 vs. 30 days (difference: 2.540 ± 7.292, 95% CI: -15.16 to 20.24, $p = 0.9279$). (**e**) $EdU^+/ASPA^+$ density in the mPFC over time; one-way ANOVA ($F_{2,18} = 7.209$, $p = 0.005$) with Sidak's *post hoc* tests comparing 7 vs. 14 days (difference: -0.5957 ± 0.5125, 95% CI: -1.846 to 0.6543, $p = 0.4529$) and 7 vs. 30 days (difference: -1.817 ± 0.4975, 95% CI: -3.031 to -0.6038, $p = 0.0036$). Representative images of $GFP^+/MBP^+/ASPA^+$ myelinating OLs (**f**, arrows) and $GFP^+/MBP^-/ASPA^-$ pre-myelinating OLs (**g**, arrowheads) in the mPFC at 30 days post-conditioning. For all panels, n = 6 mice (7 days), 9 mice (14 days), and 7 mice (30 days). Scale bars: 50 μm (**b-c**), 10 μm (**f-g**). For box-and-whisker plots, the center, boxes, and whiskers represent the median, interquartile range, and the 10^{th} and 90^{th} percentiles, with asterisks indicating the following p-value ranges: ** ≤ 0.01.

Chapter 3: Remote fear memory is impaired in the absence of new myelin formation

Inhibition of new myelin formation impairs remote fear memory recall.

As reported previously, conditional deletion of the transcription factor *Myrf* in OPCs arrests their differentiation and prevents the expression of myelin structural genes[15,17,30]. Administration of tamoxifen to adult *Myrf*$^{loxP/loxP}$ animals crossed with the *NG2CreERT* line therefore results in inhibition of oligodendrogenesis and new myelin formation while preserving existing myelinated circuits. We confirmed that this approach inhibits new myelin formation by examining the mPFC of *Myrf*$^{loxP/loxP}$*;tau-mGFP*$^{loxP/loxP}$*;NG2CreERT*$^{+/-}$ and *Myrf*$^{loxP/+}$*;tau-mGFP*$^{loxP/loxP}$*;NG2CreERT*$^{+}$ littermates. 51 days post-tamoxifen, *Myrf*$^{loxP/+}$*;tau-mGFP*$^{loxP/loxP}$*;NG2CreERT*$^{+}$ controls had many GFP^{+}/MBP^{+} mature OLs with distinctive myelinating morphology, whereas the mPFC of *Myrf*$^{loxP/loxP}$*;tau-mGFP*$^{loxP/loxP}$*;NG2CreERT*$^{+/-}$ animals, with both copies of *Myrf* deleted, contained largely GFP^{+}/MBP^{-} pre-myelinating OLs (Figure 3.1c-d).

We then generated cohorts of *Myrf*$^{loxP/loxP}$*;NG2CreERT*$^{+}$ and *Myrf*$^{loxP/loxP}$*;NG2CreERT*$^{-}$ littermate controls (hereafter referred to as *Myrf* icKO and cre-negative controls) and subjected them to contextual fear conditioning three weeks following five consecutive days of daily tamoxifen administration, assessing their freezing responses at recent and remote time points (Figures 3.1a). While both cre-negative and *Myrf* icKO animals exhibited high levels of freezing during recent retrieval sessions, context-elicited freezing responses in *Myrf* icKO mice declined over time and diverged from controls at 30 days post-conditioning, indicating a specific deficit in remote memory (Figures 3.1e).

To rule out the possibility that inhibition of basal myelin formation during the three weeks prior to conditioning has an effect on fear learning, we conducted identical fear conditioning experiments where we instead administered tamoxifen either five days pre-conditioning or just after 24 hour recall to solely inhibit new myelin formation during the consolidation period (Figures 3.1b). These *Myrf* icKO animals similarly exhibited a freezing deficit 30 days post-conditioning, suggesting that it is new myelin formation during consolidation that is important for remote memory (Figures 3.1f). We then re-conditioned these animals by administering foot shocks in the original conditioning context 31 days post-conditioning. Both *Myrf* icKO and cre-negative control animals exhibited high levels of freezing 24 hours following re-conditioning, demonstrating that there is no generalized impairment of freezing in *Myrf* icKOs at remote time points (Figure 3.1g).

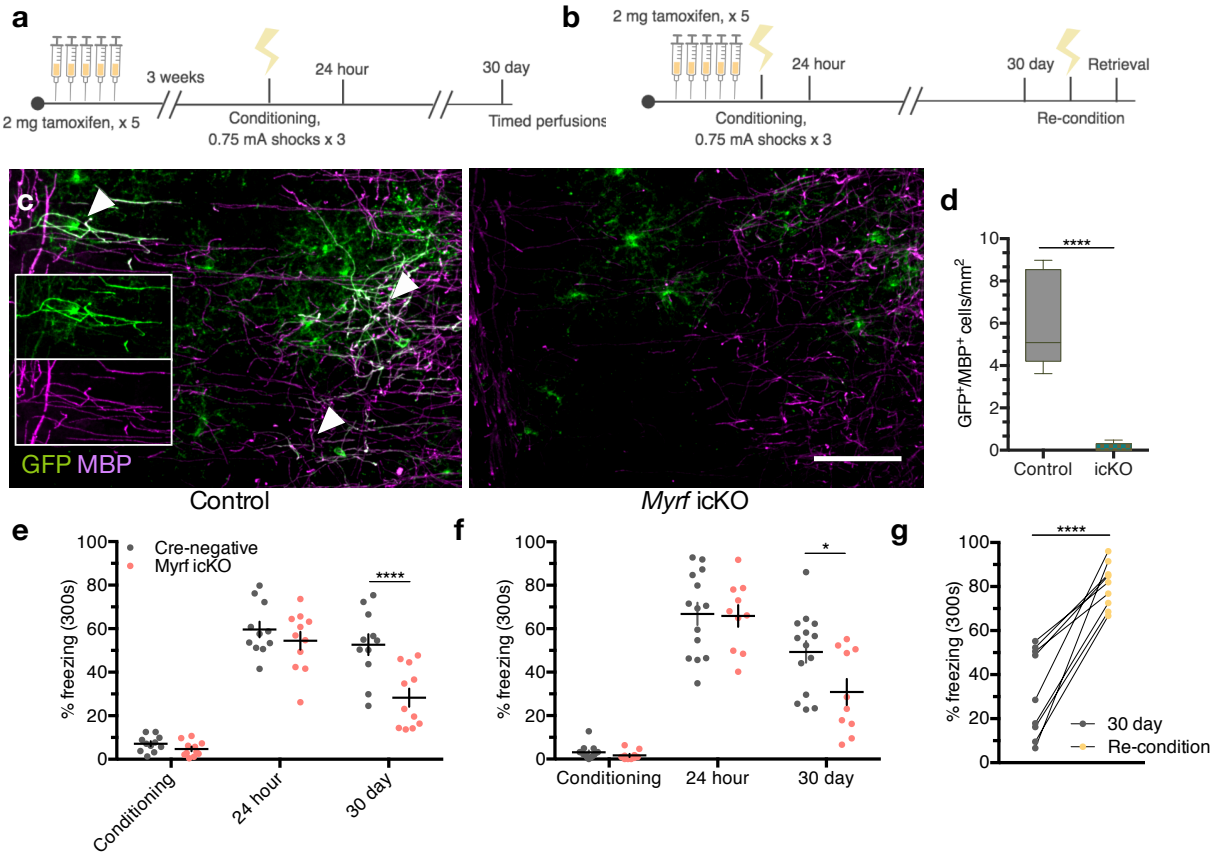

Figure 3.1. Inhibition of new myelin formation impairs remote fear memory recall.
(**a**) Experimental paradigm for contextual fear conditioning with tamoxifen administered three weeks pre-conditioning. (**b**) Experimental paradigm for contextual fear conditioning with tamoxifen administered five days prior and re-conditioning. (**c**) Representative images of GFP (green) and MBP (magenta) staining in the mPFC of *Myrf*$^{loxP/+}$*;tau-mGFP*$^{loxP/loxP}$*;NG2CreERT*$^{+}$ (left, control) animals and in *Myrf*$^{loxP/loxP}$*;tau-mGFP*$^{loxP/loxP}$*;NG2CreERT*$^{+}$ (right, *Myrf* icKO) animals 30 days post-conditioning; inset depicts separate color channels for representative GFP^{+}/MBP^{+} cell (top-most). (**d**) Quantification of GFP^{+}/MBP^{+} cell density in the mPFC of control and *Myrf* icKO animals 30 days post-conditioning; n = 6 mice per condition (control, *Myrf* icKO), unpaired two-tailed t-test (difference: -5.806 ± 0.9062, 95% CI: -7.825 to -3.786, t_{10} = 6.406, p < 0.0001). Individual fear expression over time for *Myrf* icKO and control animals administered tamoxifen three weeks (**e**) and five days (**f**) prior to conditioning; (**e**) two-way ANOVA ($F_{4,80}$ = 3.437, p = 0.0121) with Sidak's *post hoc* tests comparing cre-negative vs. *Myrf* icKO during conditioning (difference: -2.416 ± 5.790, 95% CI: -17.58 to 12.74, p = 0.9965), 24 hour (difference: -5.169 ± 5.790, 95% CI: -20.33 to 9.991, p = 0.9040), and 30 day (difference: -24.37 ± 5.790, 95% CI: -39.53 to -9.209, p = 0.0003), n = 11 mice per genotype; (**f**) two-way ANOVA ($F_{4,80}$ = 1.435, p = 0.2291) with Sidak's *post hoc* tests comparing cre-negative vs. *Myrf* icKO during conditioning (difference 1.467 ± 7.398, 95% CI: -13.19 to 16.13, p = 0.8431), 24 hour (difference: 0.9199 ± 7.398, 95% CI: -13.74 to 15.58, p = 0.9013), and 30 day (difference: 18.43 ± 7.398, 95% CI: 3.767 to 33.09, p = 0.0142), n = 14 cre-negative and 10 *Myrf* icKO mice. (**g**) Freezing responses for *Myrf* icKO animals from cohort in (**f**) 24 hours after being re-conditioned 31 days post-conditioning; paired two-tailed t-test (difference: 48.76 ± 6.624, 95% CI: 33.48 to 64.04, t_8 = 7.361, p < 0.0001). Scale bar: 50 μm. For box-and-whisker plots, the center, boxes, and whiskers represent the median, interquartile range, and the 10th and 90th percentiles. For dot plots, data are presented as mean ± SEM, with asterisks indicating the following p-value ranges: * ≤ 0.05, **** ≤ 0.0001.

Chapter 4: Fear-associated neurophysiology is abnormal in the absence of new myelin formation

Immediate early gene expression following remote memory recall is impaired in the absence of new myelin formation

To assess neuronal activity in response to remote memory recall, we perfused *Myrf* icKO and cre-negative control animals ninety minutes following the 30-day retrieval session and conducted histological analysis of Fos induction in a number of fear-associated brain regions. We found that the density of Fos^+ cells was significantly decreased in the PL and IL of the mPFC, BLA, and dHPC of *Myrf* icKOs compared to cre-negative controls (Figure 4.1a, c-e), with the degree of Fos induction displaying a linear relationship with individual freezing at 30 days post-conditioning (Figure 4.1g-j). Notably, Fos induction was similar across genotypes in home cage controls at 30 days post-conditioning (Figure 4.1b) and following recent memory retrieval at 24 hours post-conditioning (Figure 4.1f). Fos^+ cell density was also similar in a non-fear associated brain region, the somatosensory cortex (SSC), across genotypes (Figure 4.1a). This indicates that the physiological response of neurons within the fear memory network is specifically impaired in the absence of myelin formation during remote memory recall.

Population calcium dynamics in the medial prefrontal cortex are altered in the absence of new myelin formation.

In order to relate neuronal activity to freezing behavior in *Myrf* icKOs and cre-negative controls with high temporal resolution, we performed fiber photometry recordings in freely behaving mice during contextual fear conditioning and retrieval sessions (Figures 4.2a). We injected adeno-associated viral (AAV) vectors expressing the calcium indicator GCaMP6f and implanted optical fibers at the PL/IL border of the mPFC (Figure 4.2b-c). This targeting effectively records from

the IL, where suppression of firing of mPFC units in response to conditioned cues has previously been reported[31,32].

Following recovery from the surgery, animals were administered tamoxifen for five days, rested for three weeks, and then subjected to contextual fear conditioning (Figure 4.2a). Both control and *Myrf* icKOs animals displayed robust neuronal responses to foot shock in the mPFC, with no difference in shock-evoked activity between genotypes (Figure 4.2d-e, h). To determine whether recall-induced neuronal activity was altered in the absence of new myelin formation, we aligned photometry signals to behavioral footage during retrieval sessions and analyzed the changes in mPFC activity during transitions from mobility to freezing. (Figure 4.2f-g). In line with previous reports conducting electrophysiological recordings of IL units [31,32], we found that, at 24 hours post-conditioning, mPFC activity was suppressed during fear memory recall in both control and *Myrf* icKO animals (Figures 4.2g, 4.2i). However, we found that prefrontal dynamics associated with fear recall evolved over time in control animals, which exhibited an elevation of mPFC activity during transitions from mobility to freezing at 30 days post-conditioning (Figures 4.2g, i). This time-dependent change in the recall-associated response was not evident in *Myrf* icKO animals, which continued to show a suppression of prefrontal activity during freezing transitions at 30 days post-conditioning (Figures 4.2g, i). The absence of this temporal evolution of prefrontal dynamics in *Myrf* icKO animals suggests that active oligodendrogenesis is required for remote fear memory consolidation.

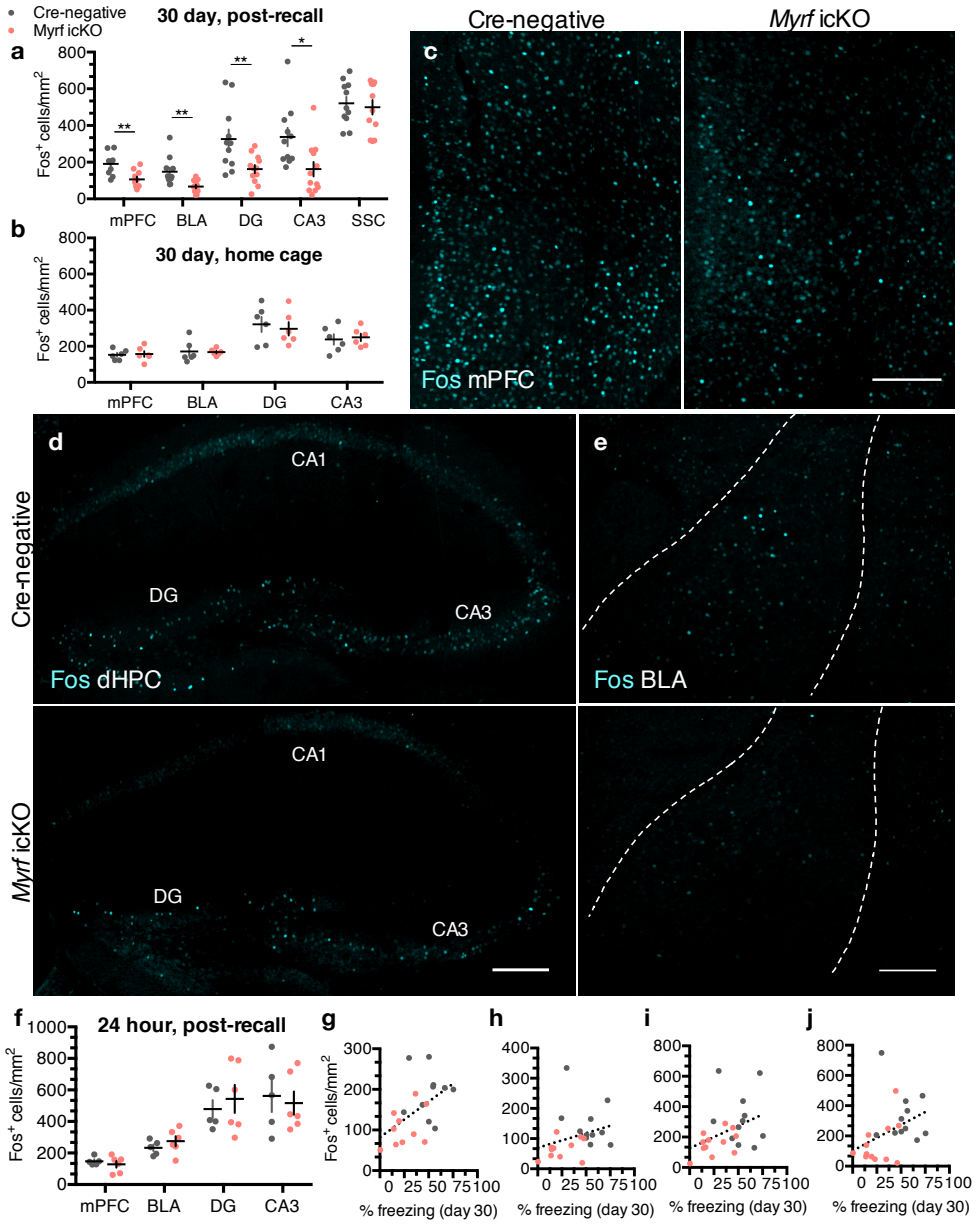

Figure 4.1. Immediate early gene expression following remote recall is impaired in the absence of new myelin formation. (**a**) Quantification of Fos$^+$ cell density across brain regions following 30-day retrieval sessions in *Myrf* icKO vs. cre-negative controls; unpaired two-tailed t-tests, mPFC (difference: 84.27 ± 23.89, 95% CI: - 34.09 to 134.5, t_{21} = 3.528, p = 0.0024), BLA (difference: 80.55 ± 24.87, 95% CI: 28.66 to 132.4, t_{21} = 3.238, p = 0.0041), DG (difference: 163.5 ± 55.29, 95% CI: 48.50 to 278.5, t_{21} = 2.957, p = 0.0075), CA3 (difference: 175.4 ± 63.83, 95% CI: 42.70 to 308.2, t_{21} = 2.749, p = 0.012), SSC (difference: 21.86 ± 53.48, 95% CI: -89.35 to 133.1, t_{21} = 0.4088, p = 0.6868), n = 12 cre-negative and 11 *Myrf* icKO mice. (**b**) Quantification of baseline home cage Fos$^+$ cell density across brain regions in *Myrf* icKO vs. cre-negative controls; unpaired two-tailed t-tests, mPFC (difference: 4.591 ± 19.85, 95% CI: -39.64 to 48.82, t_{10} = 0.2313, p = 0.8218), BLA (difference: -3.475 ± 25.49, 95% CI: -60.28 to 53.33, t_{10} = 0.1363, p = 0.8943), DG (difference: -24.73 ± 56.36, 95% CI: -150.3 to 100.8, t_{10} =

0.4387, p = 0.6702), CA3 (difference: 11.42 ± 36.00, 95% CI: -68.79 to 91.63, t_{10} = 0.3172, p = 0.7576), n = 6 mice per genotype. Representative images of Fos induction (cyan) in the mPFC (**c**), dHPC (**d**), and BLA (**e**) of cre-negative and *Myrf* icKO animals following 30-day retrieval. (**f**) Quantification of Fos$^+$ density across brain regions following 24-hour retrieval sessions; unpaired two-tailed t-tests, mPFC (difference: -18.95 ± 25.61, 95% CI: -76.90 to 38.99, t_9 = 0.74, p = 0.4781), BLA (difference: 41.33 ± 39.72, 95% CI: -48.53 to 131.2, t_9 = 1.041, p = 0.3252), DG (difference: 64.80 ± 111.0, 95% CI: -186.2 to 315.8, t_9 = 0.5839, p = 0.5736), CA3 (difference: -45.58 ± 123.5, 95% CI: -324.9 to 233.7, t_9 = 0.3692, p = 0.7205), n = 5 cre-negative and 6 *Myrf* icKO mice. Individual 30 day freezing responses plotted against Fos$^+$ cell density in mPFC (**g**), BLA **(h**), DG **(i**), and CA3 **(j**); two-tailed Spearman's correlation test, mPFC (R_s = 0.589, 95% CI: 0.1853 to 0.8231, p = 0.0062), BLA (R_s = 0.467, 95% CI: 0.04322 to 0.7483, p = 0.0284), DG (R_s = 0.451, 95% CI: 0.03545 to 0.7343, p = 0.305), CA3 (R_s = 0.535, 95% CI: 0.1449 to 0.7812, p = 0.0085), n = 23 mice. Scale bars: 200 µm (**c-e).** Data are presented as mean ± SEM, with asterisks indicating the following p-value ranges: * ≤ 0.05, ** ≤ 0.01.

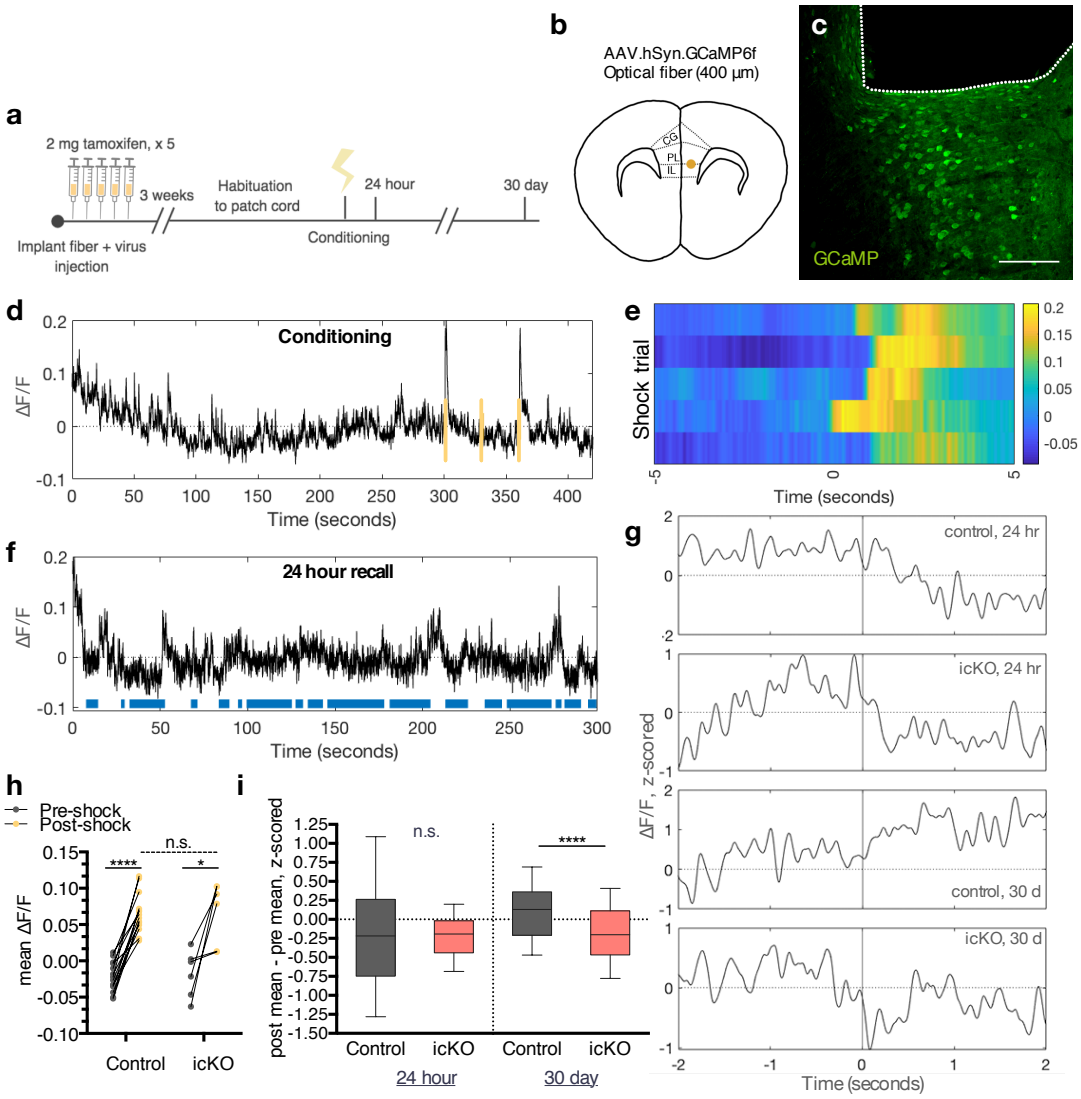

Figure 4.2. Prefrontal population calcium dynamics in the medial prefrontal cortex are altered in the absence of new myelin formation. (**a**) Experimental paradigm for surgeries, tamoxifen administration, and fiber photometry recordings during contextual fear conditioning and retrieval. (**b**) Schematic and anatomical location for delivery of calcium indicator and optical fiber and (**c**) representative image of GCaMP expression (green) and fiber placement in the mPFC. (**d**) Representative ΔF/F trace across a conditioning session with foot shocks overlaid in yellow. (**e**) Heatmap of ΔF/F values five seconds pre- and post-shock for the first shock delivered in five representative animals, color map represents ΔF/F. (**f**) Representative ΔF/F trace across a 24-hour retrieval session with freezing overlaid in blue. (**g**) Representative z-scored ΔF/F traces across a time window spanning two seconds pre- and post-bout transition, from top to bottom: control, 24 hours; *Myrf* icKO, 24 hours; control, 30 days; *Myrf* icKO, 30 days. (**h**) Quantification of the mean ΔF/F during the five seconds pre- and post-shock, stratified by genotype; n = 14 bouts bouts/7 mice (control) and 6 bouts/3 mice (*Myrf* icKO); paired two-tailed t-tests comparing pre- and post-shock for control (difference: 0.08767 ± 0.007947, 95% CI: 0.07051 to 0.1048, t_{13} = 11.03, p < 0.0001) and *Myrf* ickO (difference: 0.08468 ± 0.02609, 95% CI: 0.01760 to 0.1518, t_5 = 3.245, p = 0.0031) animals; unpaired two-tailed t-test comparing post across genotypes (difference: 0.001432 ± 0.01574, 95% CI: -0.03163 to 0.03449, t_{18} = 0.09098, p = 0.9285). (**i**) Quantification of the difference between the z-scored mean ΔF/F of the two seconds pre- and post-bout transition for control and *Myrf* icKO animals, plotted during 24-hour (left bars) and 30-day (right bars) retrieval; n = 10 bouts for 7 mice (control) and 7 mice (*Myrf* icKO); unpaired two-tailed t-tests comparing across genotypes at 24 hour (difference -0.02001 ± 0.1516, 95% CI: -0.3192 to 0.2792, t_{138} = 0.132, p = 0.8951) and 30 day (difference: -0.2963 ± 0.07301, 95% CI: -0.4403 to -0.1524, t_{138} = 4.5059, p < 0.0001). Scale bar: 100 μm**.** For box-and-whisker plots, the center, boxes, and whiskers represent the median, interquartile range, and the 10th and 90th percentiles, with asterisks indicating the following p-value ranges: n.s. (not significant) > 0.05, ** ≤ 0.01, **** ≤ 0.0001.

Chapter 5: Pharmacological induction of new myelin formation preserves remote fear memory

Inducing new myelin formation preserves retrieval of a contextual fear memory

Clemastine fumarate is an anti-muscarinic compound identified as a pro-myelinating agent in high throughput screening efforts to find therapeutics for demyelinating disease[33,34]. Administration of clemastine to humans and rodents with inflammatory demyelination promotes remyelination and relieves the severity of clinical symptoms[35,36]. Clemastine additionally promotes myelination and rescues behavioral deficits in mice that are hypomyelinated following either prolonged social isolation or chronic hypoxia[36,37]. To determine if induction of new myelin formation impacts fear memory, we subjected cohorts of wildtype 8-week old male C57BL/6J mice to contextual fear conditioning while injecting them daily with either clemastine or vehicle from 3 days pre- to 21 days post-conditioning (Figures 5.1a). We verified that chronic clemastine administration increases new myelin formation under healthy, physiological conditions by observing increased $ASPA^+$ cell density and mean MBP fluorescence intensity in the mPFC of clemastine-treated mice (Figure 5.1b-d).

Nonetheless, clemastine-treated mice displayed persistent and high freezing responses over time, suggesting that increasing new myelin formation stabilizes remote fear memory (Figure 5.1e). To rule out the possibility that a remote memory phenotype is not simply a result of prolonged clemastine treatment, we administered daily clemastine for three weeks prior to conditioning and observed normal freezing behavior during recent memory recall (Figure 5.1f-g). Finally, we administered vehicle or clemastine injections to *Myrf* icKO mice and subjected them to the contextual fear learning paradigm (Figure 5.1h). In the absence of new myelin formation, clemastine-treated *Myrf* icKO animals appear identical to vehicle-treated animals (Figure 5.1i),

indicating that the effects of clemastine on fear memory are specifically dependent on new myelin formation. Collectively, these results indicate that inducing new myelin formation preserves remote fear memory, but may potentially decrease its precision.

We then perfused vehicle- and clemastine-treated animals ninety minutes after the 30-day retrieval session for subsequent histological analysis of immediate early gene expression. Fos^{+} cell density was increased in clemastine-treated animals in the mPFC, BLA, and dHPC but not the SSC (Figure 5.2a-c). However, no differences in Fos induction were detected following recent memory recall in mice pre-treated with three weeks of clemastine, nor following remote memory recall in home cage mice that never learned the fear association (Figure 5.2d-e) These results suggest that population neuronal activity in response to conditioned cues is increased in fear-associated brain regions following chronic clemastine administration.

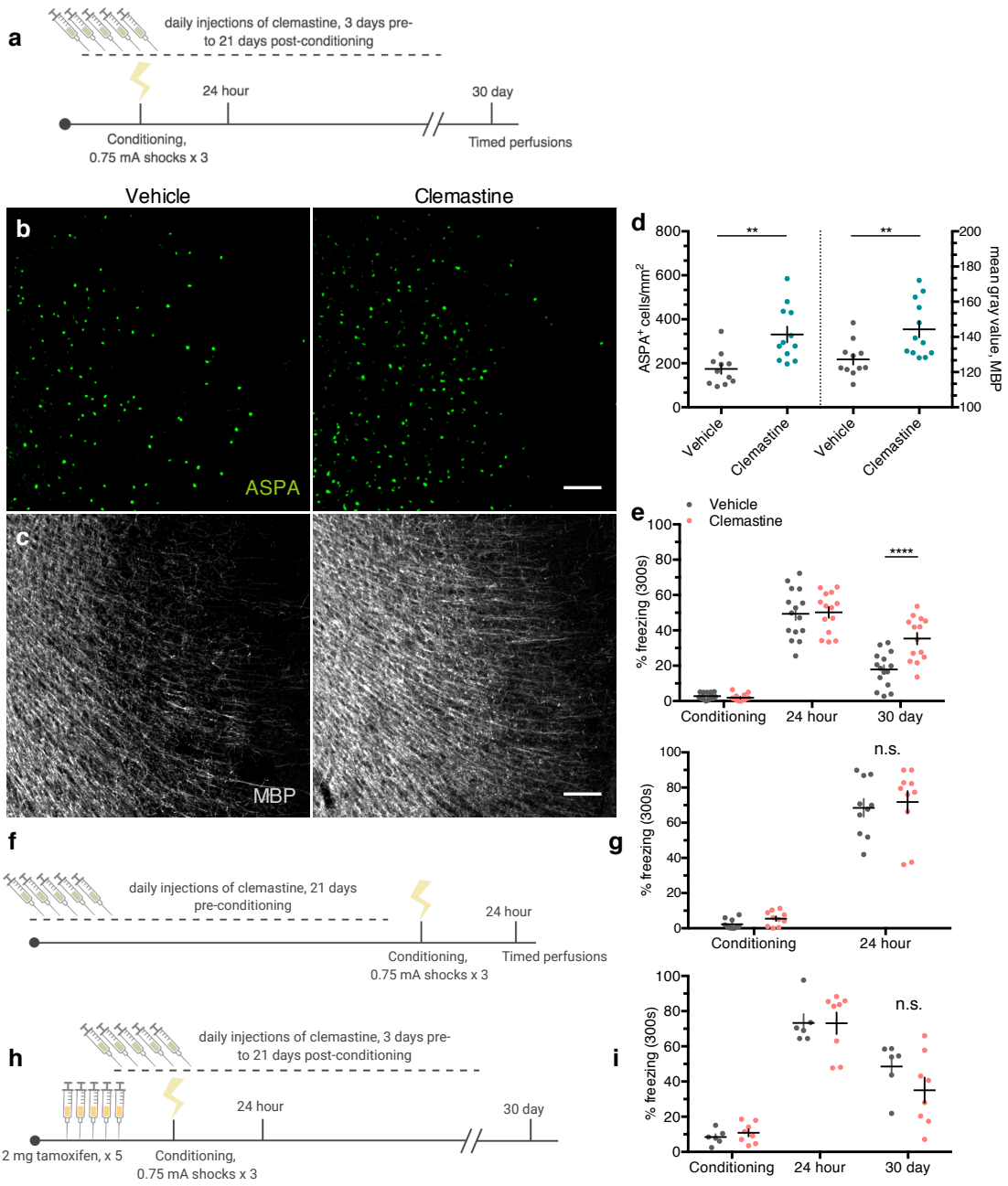

Figure 5.1. Induction of new myelin formation preserves remote fear memory recall. (**a**) Experimental paradigm for clemastine injections and contextual fear conditioning. Representative images of ASPA (green) and MBP (gray) signal in the mPFC of vehicle- (**b**) and clemastine-treated (**c**) animals 30 days post-conditioning. (**d**) Quantification of ASPA$^+$ cell density (left bars) and MBP mean fluorescence (right bars) in the mPFC of vehicle- and clemastine-treated animals; unpaired two-tailed t-tests comparing vehicle versus clemastine for ASPA$^+$ density (difference: 156.9 ± 43.21, 95% CI: 67.00 to 246.7, t_{21} = 3.63, p = 0.0016) and MBP fluorescence (difference: 17.10 ± 5.640, 95% CI: 5.370 to 28.83, t_{21} = 3.032, p = 0.0063), n = 11 vehicle and 12 clemastine mice. (**e**) Individual fear expression over time for vehicle- and clemastine-treated animals; two-way ANOVA ($F_{4,108}$ = 5.884, p = 0.0003) with Sidak's *post hoc* tests comparing across treatment groups for conditioning (difference: 0.8941 ± 4.116, 95% CI: -

9.860 to 11.65, p = 0.9928), 24 hour (difference: -0.8004 ± 4.116, 95% CI: -11.55 to 9.954, 0.9948), and 30 day (difference: -17.49 ± 4.116, 95% CI: -16.00 to -0.3832, p = 0.0002), n = 15 vehicle and 14 clemastine mice. (**f**) Experimental timeline controlling for the duration of clemastine injections, in which the entire injection protocol is completed prior to initiation fear conditioning and recent memory recall, n = 10 mice per treatment. (**g**) Individual freezing responses during recent memory recall testing for animals pre-treated with clemastine in experimental timeline (**f**); two-way ANOVA ($F_{1,18}$ = 0.0003928, p = 0.9844). (**h**) Experimental paradigm for clemastine injections in *Myrf* icKO animals. (**i**) Individual fear expression over time for vehicle- and clemastine-treated *Myrf* icKO animals; two-way ANOVA ($F_{4,48}$ =1.357, p = 0.2629), n = 6 vehicle and 8 clemastine mice. Scale bars: 100 μm (**b-c**). Data are presented as mean ± SEM, with asterisks indicating the following p-value ranges: ** ≤ 0.01, **** ≤ 0.0001.

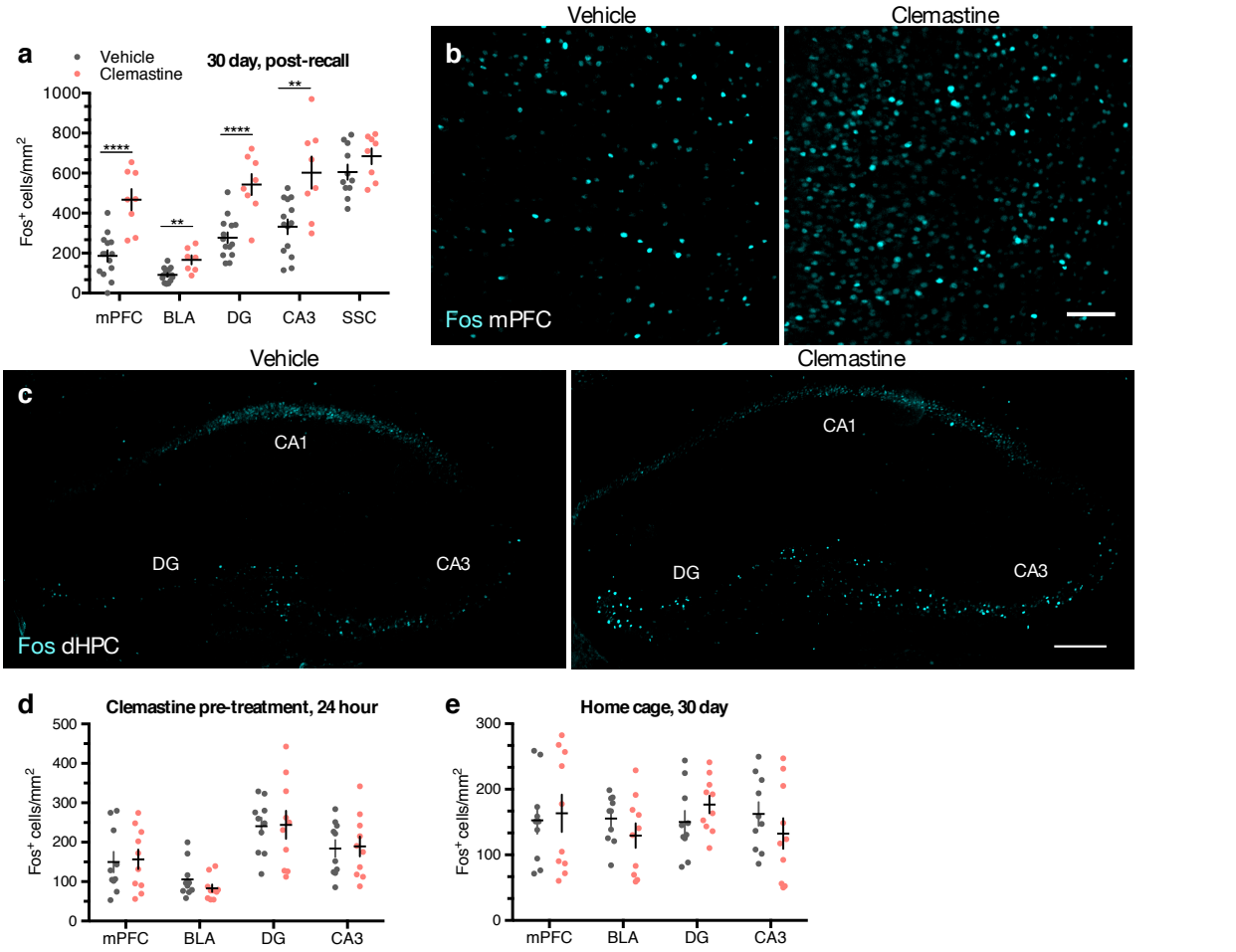

Figure 5.2. Induction of new myelin formation increases immediate early gene expression following remote fear memory recall. (**a**) Quantification of Fos^+ cell density across brain regions in vehicle- and clemastine-treated animals following 30-day retrieval; unpaired two-tailed t-tests, mPFC (difference: 280.7 ± 54.50, 95% CI: 167.0 to 394.4, t_{19} = 5.15, p < 0.0001), BLA (difference: 75.06 ± 20.12, 95% CI: 32.95 to 117.2, t_{19} = 3.73, p = 0.0014), DG (difference: 268.7 ± 56.69, 95% CI: 150.0 to 387.3, t_{19} = 4.739, p < 0.0001), CA3 (difference: 270.5 ± 77.34, 95% CI: 109.2 to 431.8, t_{19} = 3.497, p = 0.0023), SSC (difference: 79.25 ± 55.73, 95% CI: -38.33 to 196.8, t_{19} = 1.422, p = 0.1731), n = 13 vehicle and 8 clemastine mice. Representative images of Fos induction (cyan) in the mPFC (**b**) and dHPC (**c**) of vehicle- and clemastine-treated animals following 30-day retrieval. (**d**) Quantification of Fos^+ cell density across brain

regions in vehicle- and clemastine pre- treated animals, represented in Figure 7g-f, following 24 hour retrieval; unpaired two-tailed t-tests, mPFC (difference: 6.885 ± 35.98, 95% CI: -68.71 to 82.48, t_{18} = 0.1913, p = 0.8504), BLA (difference: -22.53 ± 17.11, 95% CI: -58.48 to 13.42, t_{18} = 1.317, p = 0.2045), DG (difference: 3.547 ± 41.64, 95% CI: -83.94 to 91.04, t_{18} = 0.08518, p = 0.9331), CA3 (difference: 5.178 ± 33.28, 95% CI: -64.74 to 75.10, t_{18} = 0.1556, p = 0.8781), n = 10 mice per treatment group. (**e**) Quantification of Fos^+ cell density across brain regions in home cage vehicle- and clemastine-treated animals, represented in Figure S6a, g, in the absence of fear learning; unpaired two-tailed t-tests, mPFC (difference: 10.88 ± 35.04, 95% CI: -62.73 to 84.50, t_{18} = 0.3106, p = 0.7597), BLA (difference: -25.98 ± 22.03, 95% CI: -72.27 to 20.31, t_{18} = 1.179, p = 0.2537), DG (difference: 26.58 ± 21.51, 95% CI: -18.61 to 71.77, t_{18} = 1.236, p = 0.2324), CA3 (difference: -29.91 ± 29.50, 95% CI: -91.88 to 32.06, t_{18} = 1.014, p = 0.3239), n = 10 mice per treatment group. Scale bars: 100 μm (**b**), 200 μm (**c**)**.** Data are presented as mean ± SEM, with asterisks indicating the following p-value ranges: ** ≤ 0.01, **** ≤ 0.0001.

Chapter 6: Conclusion & future directions

Conclusion

In this study, we demonstrate that the generation of new oligodendrocytes is required for the proper functioning of neural circuits that mediate remote fear memory. This process is specific to remote memory, as *Myrf* icKO mice appear identical to cre-negative control animals at recent time points by many metrics, including freezing behavior, immediate early gene expression, and mPFC population calcium dynamics during both conditioning and recent retrieval sessions. Furthermore, these behavioral and neurophysiological deficits manifest after several weeks, suggesting that it is the formation of new myelin, which occurs over a timescale of weeks as we have described here, and not oligodendrocyte differentiation *per se*, which occurs over a timescale of hours[17], that is important for remote fear memory recall. In addition to our electron microscopy analyses, we verify that in the healthy adult brain, ASPA is an exclusive marker for mature, myelinating OLs extruding MBP^+ processes with characteristic morphology of compact myelin sheaths. Thus, we are able to demonstrate that fear learning induces the formation of *bona fide* new myelin in the prefrontal cortex.

In two seminal studies, *Myrf* icKO mice displayed impairments in learning to run on a complex wheel as early as several hours into training. This rapid learning deficit was correlated with the immediate differentiation of OPCs into immature OLs within this same time window[15,17]. In contrast, the onset of deficits we have observed occurs much more slowly, reflecting the time required for compact myelin formation in the adult brain. Learning impairment on a more rapid timescale may conceivably be due to a loss of non-myelinating functions of OLs, such as metabolic support, neurotransmitter homeostasis, or clustering of voltage-gated ion channels[39,40,41,42]. Alternatively, the three-week interim between tamoxifen administration and

presentation of the complex wheel in which basal myelin formation is inhibited may impact learning performance independently of experience-induced OL production. In our study, we have presented evidence against the latter possibility by observing fear learning deficits in *Myrf* icKO animals administered tamoxifen both immediately prior to and after fear conditioning.

Remote memory consolidation, or systems consolidation, involves a reorganization of memory networks, over the course of several weeks or longer, such that retrieval of a memory transitions from dependence on the hippocampus to distributed cortical ensembles over time[28,29]. However, the synaptic, cellular, and circuit-level mechanisms that underlie this process are not well understood. On the basis of lesioning studies, immediate early gene expression, and functional optogenetics experiments, the mPFC is thought to be particularly important for remote memory[24,25,43,44]. We affirm this in our experiments by recording from a population of neurons over the course of a month, as a memory transitions from recent to remote, and demonstrating that the population response of the mPFC to identical context cues evolves over time, which, to our knowledge, has not been achievable with traditional electrophysiological recording methods. These findings are consistent with miniaturized microscopy imaging of the mPFC during fear conditioning, which indicate that a small subset of shock-responsive cells elevate their firing rates 15 days post-conditioning when an animal is placed in the conditioned context[25]. Remarkably, this temporal evolution is not observed in the absence of new myelin formation, which, in conjunction with deficits in freezing behavior and immediate early gene expression specifically during remote recall, suggests that systems consolidation requires active myelination.

We observe fear learning-induced changes in myelin content specifically in the mPFC but network-wide changes in immediate early gene expression, consistent with previous characterizations demonstrating that manipulating activity in a single node can have widespread

effects on fear memory circuits[27]. Although the mPFC is dispensable for recent memory, input from the entorhinal cortex and BLA to the mPFC at the time of conditioning is required for the initial establishment of neuronal ensembles that subsequently mature to mediate remote memory retrieval[25]. Here, we describe an analogous situation in which OPC proliferation in the mPFC is elicited immediately at the time of conditioning, but the ensuing maturation of myelinating OLs occurs over a prolonged period that is similar in length to the approximate timeline reported for systems consolidation. Notably, we detected an increase in post-training proliferation of OPCs in the BLA that did not translate to an increase in myelinating OLs several weeks later, suggesting that these OPCs may have differentiated but failed to mature. This is in accordance with longitudinal two photon imaging of OPC dynamics[3] and suggests that, although memory acquisition is important to initiate this sequence of events, it is perhaps stable integration of maturing OLs during the consolidation period that is the important regulatory point in experience-dependent myelination.

Future directions

The mechanistic details of how new myelin formation acts to support remote memory is a salient question and requires a thorough understanding of how neuronal ensembles act in concert to achieve memory consolidation and retrieval. Though this remains an active area of research, several points appear to be true: 1) systems consolidation involves substantial interregional reorganization of neuronal networks in the form of neuronal engram ensembles[24,25,28,43,44]; 2) active interregional communication between brain regions separated in space, arbitrated by the myelinated axons of projection neurons, is required for both successful memory consolidation and retrieval[24,25,27,45,46,47,48]; 3) this interregional communication seems to be characterized by a high degree of temporal precision, particularly in the form of synchronized oscillatory activity[46,47]. Thus, there are several conceivable ways through which new myelin formation can interact with or complement neural circuits to support systems consolidation and remote

memory retrieval. Myelination could be strengthening specific projections in a manner akin to Hebbian plasticity, facilitating communication between spatially distributed neuronal ensembles, and/or tuning axonal conduction velocities such that synchronized oscillations or other computationally relevant firing patterns can be achieved[20,48]. A recent study reported episodic memory deficits and disruptions in ripple-spindle coupling between the mPFC and dHPC several days after tamoxifen administration in *Myrf* icKO animals[49]. While the timing of these observations is much more rapid than the timeline required for new, compact myelin formation that we have described here, ripple-spindle coupling represents a fascinating example of a memory consolidation mechanism requiring temporally precise interregional coordination and active oligodendrogenesis[47,49]. Collectively, these results indicate that experience-dependent oligodendrocyte production may impact circuit function through multiple mechanisms and across different time scales. Distinguishing between and elaborating on these many potential scenarios represents a major technical challenge and will likely require the development of tools for region- or projection-specific manipulations of new myelin formation in conjunction with recordings of neuronal ensembles across multiple brain regions in freely behaving animals.

In addition to establishing that remote fear memory requires new myelin formation, we demonstrate that induction of new myelin formation via clemastine enhances remote fear memory. As clemastine administration had no effect in *Myrf* icKO animals, this effect is likely dependent on new myelin formation. Notably, magnetic resonance imaging (MRI) examination of combat veterans with PTSD suggests increased hippocampal myelin content compared to combat-exposed controls, putatively implicating aberrant myelin formation in the pathophysiology of PTSD[50]. Although PTSD involves a constellation of symptoms, one of its prominent features is intense and overgeneralized fear responses[21], which we have reproduced, to some degree, in mice chronically treated with clemastine. Indeed, a cardinal property of newly formed myelin is its stability, which may be desirable for retaining adaptive memories and

learned skills, but detrimental if maladaptive fear responses are persistent and generalized to everyday situations[1,2,18].Thus, investigating the role of new myelin formation in adaptive and maladaptive learning constitutes an important opportunity both for understanding, diagnosing, and potentially treating PTSD and other neuropsychiatric illnesses, and for elucidating fundamental mechanisms of learning and memory.

Chapter 7: Materials & Methods

Mice

Myrf$^{loxP/loxP}$ (JAX: 010607) mice were crossed to the *NG2-CreERT* (JAX: 008538) line to generate *Myrf*$^{loxP/loxP}$; *NG2-CreERT* (Myrf icKO) mice. These lines were maintained through crosses of *Myrf*$^{loxP/loxP}$*;NG2CreERT*$^{+}$ and *Myrf*$^{loxP/loxP}$*; NG2CreERT*$^{+}$ breeders, generating *Myrf*$^{loxP/loxP}$*;NG2CreERT*$^{+}$ and *Myrf*$^{loxP/loxP}$*; NG2CreERT*$^{-}$ littermates on a mixed 129; CBA/J; C57BL/6J background. To validate inhibition of new myelin formation following *Myrf* deletion, triple transgenic *Myrf*$^{loxP/loxP}$*;tau-mGFP*$^{loxP/loxP}$ (JAX: 21162)*;NG2CreERT*$^{+}$ *and Myrf*$^{loxP/+}$*;tau-mGFP*$^{loxP/loxP}$*;NG2CreERT*$^{+}$ male and female littermates were generated through crosses of *Myrf*$^{loxP/loxP}$*;tau-mGFP*$^{loxP/loxP}$*;NG2CreERT*$^{+}$ *and Myrf*$^{loxP/+}$*;tau-mGFP*$^{loxP/loxP}$*;NG2CreERT*$^{-}$ breeders. Cre-mediated recombination was induced via daily intraperitoneal injections of 20 mg/ml tamoxifen (Sigma-Aldrich) dissolved in 10% ethanol/90% peanut oil for five consecutive days, at a dose of 80 mg/kg. Mice were rested for either three weeks or five days before beginning subsequent behavioral experiments. *Tau-mGFP*$^{loxP/loxP}$*;NG2CreERT*$^{+}$ mice on a C57BL/6J background were maintained through crosses of *tau-mGFP*$^{loxP/loxP}$*;NG2CreERT*$^{+}$ and *tau-mGFP*$^{loxP/loxP}$*;NG2CreERT*$^{-}$ breeders. All transgenic mice used in this study were littermates aged 8 - 10 weeks at the start of experiments. Males and females were used in approximately equal numbers and age-matched littermates were randomly assigned to cohorts. Genotyping was performed as recommended on the Jackson Laboratories datasheet for each mouse line via standard polymerase chain reaction of tail-derived genomic DNA. Sequences for all genotyping primers are detailed in the key resources table.

Clemastine experiments in Figures 7-8 and 5-ethynyl-2'-deoxyuridine *(*EdU) experiments in Figures 1-2 were conducted with 8-week old male C57BL/6J mice (JAX: 000664). Clemastine

fumarate (AvaChem Scientific) was prepared as a 1 mg/ml solution in 10% dimethyl sulfoxide (DMSO; Sigma)/phosphate-buffered saline (PBS) and administered via daily intraperitoneal injection at a dose of 10 mg/kg, alternating injection sites each day. Vehicle controls were injected in an identical manner with 10% DMSO/PBS. EdU (Carbosynth) was prepared as a 10 mg/ml solution in PBS and administered via intraperitoneal injection at a dose of 80 mg/kg.

All animals were group-housed with one to four same-sex cagemates in standard rodent cages within a pathogen-free barrier facility on a 12-hour light/dark cycle, with behavioral testing and recordings performed during the light phase. Food and water were available *ad libitum* and cages were changed on a biweekly basis by veterinary technicians. All procedures were pre-approved by and conducted in accordance with the U.S. NIH Guide for the Care and Use of Laboratory Animals and the Institutional Animal Care and Use Committees at the University of California, San Francisco.

Behavior

Conditioned fear was elicited by administering three mild footshocks (0.75 mA), spaced thirty seconds apart, following a five-minute exposure to an array of contextual cues (conditioning chamber, chamber lights, white noise, scent of anise extract). Retrieval of the fear memory was assessed by re-exposure of the animal to the conditioning context in the absence of shock, and freezing, the cessation of all movement outside of respiration, was interpreted as expression of fear memory. Video recordings were acquired and scored automatically in FreezeFrame (Actimetrics). Mice were habituated to transport and holding in a separate room for at least one hour prior to all conditioning or retrieval sessions. For assessment of Fos induction following fear memory retrieval, habituation was extended to four hours and all animals were perfused exactly 90 minutes after the start of the retrieval session. For assessment of generalization, freezing was measured in a context similar to the conditioning context but with the following

variations: chamber lights and fan were turned off, scent of anise extract was swapped for lemon extract, and a plastic divider was inserted to make the chamber walls circular and opaque. Freezing in the similar context was tested two hours following retrieval testing in the original conditioning context, and animals were rested in a holding room between sessions. For the immediate shock condition, one 0.75 mA footshock was administered thirty seconds after context exposure, followed by immediate removal of the animal from the chamber.

Anxiety-like behaviors were assessed via the open field test (OFT) and elevated plus maze (EPM). Video recordings were acquired in Ethovision (Noldus) and time spent in the periphery of the OFT and in the closed arms of the EPM were scored through automated object detection, and interpreted as anxiety-like behavior. Freezing and anxiety-like behaviors were both scored via an automated, unbiased process and thus were not explicitly performed blinded.

Fiber photometry

Recombinant adeno-associated virus (AAV; AAV1.hSyn.GCaMP6f.WPRE.SV40[51]; Addgene) was stereotactically injected unilaterally into the right mPFC (+1.7 mm AP, +0.35 mm ML, -2.75/2.5/2.25/2.0 mm DV, 150 nl per injection site) of male *Myrf*$^{loxP/loxP}$*;NG2CreERT*$^{+/-}$ and *Myrf*$^{loxP/loxP}$*; NG2CreERT*$^{-/-}$ littermates. 400 μm diameter and 2.2 mm length optical fibers encased in stainless steel ferrules (Doric) were implanted directly above the injection site (-1.9 mm DV) within the same surgery. After recovery from surgery over several days, mice were administered a five-day tamoxifen regimen. Three weeks following surgery, animals were habituated to the patch cord (Doric) for thirty minutes for three consecutive days, and subjected to contextual fear conditioning as previously described. Fiber photometry recordings of mPFC calcium dynamics were acquired during each conditioning or retrieval session using the Synapse software suite (Tucker-Davis Technologies) and a hardware setup consisting of an RZ5P fiber photometry processor (Tucker-Davis Technologies), 405 nm and 465 nm LED

excitation (Doric), a 6-port fluorescence mini cube (Doric), and photoreceiver module (Doric). 465 nm and 405 nm LED excitation were sinusoidally modulated at 210 Hz and 330 Hz, respectively. Patch cord autofluorescence was bleached overnight prior to every recording session via continuous LED illumination. A five-minute baseline recording in the home cage was acquired just prior to each conditioning or retrieval session. All animals were perfused for *post hoc* histology following their final recording session to verify viral expression and implant placement. One animal was excluded from fiber photometry analysis due to incorrect fiber placement.

Immunohistochemistry

Animals were perfused with PBS followed by 4% (w/v) paraformaldehyde (PFA) in PBS. Intact brains were extracted and post-fixed in 4% PFA overnight at 4°C. The tissue was then cryoprotected in 30% (w/v) sucrose (Sigma) in PBS, sectioned at 30 µm on a sliding microtome (Leica), and stored as floating sections in PBS containing 0.02% sodium azide. For immunohistological analysis, brain sections were blocked in 10% goat or donkey serum in PBS containing 0.1 % (v/v) Triton X-100 (PBST) for 1 - 2 hours at room temperature (RT). Primary antibodies were diluted in blocking solution and incubated overnight at 4°C and secondary antibodies were diluted in PBS and incubated for two hours at RT. The primary antibodies used in this study and their working concentrations are as follows: rabbit monoclonal anti-GFP (ThermoFisher Cat#G10362, 1:1000), chicken polyclonal anti-GFP (Aves Labs Cat#GFP-1020, 1:1000), rabbit polyclonal anti-Olig2 (Millipore Cat#AB9610, 1:1000), rabbit polyclonal anti-ASPA (Sigma-Aldrich Cat#ABN1698, 1:1000), rat monoclonal anti-MBP (Serotec Cat#MCA409S, 1:200), goat polyclonal anti-Fos (Santa Cruz Antibodies Cat#sc-52-G, 1:500), rabbit polyclonal anti-Iba1 (Wako Cat#019-19741, 1:1000).

EdU incorporation by proliferating cells was detected via copper-catalyzed click chemistry with a picolyl azide conjugated to a 488 Alexa Fluor dye (Click Chemistry Tools). For co-labeling with immunohistochemical staining, free-floating brain sections were incubated with a reaction mix consisting of 488 picolyl azide (5 μM), $CuSO_4$ (Sigma-Aldrich, 4 mM), and sodium ascorbate (Acros, 100 mM) in PBS for 30 minutes at RT, between the blocking and primary antibody incubation steps.

Electron microscopy

8-week old male C57BL/6J mice were subjected to contextual fear conditioning and perfused 30 days post-conditioning with 2% (w/v) PFA/1.25% (w/v) glutaraldehyde in 0.1M sodium cacodylate buffer. Intact brains were extracted and post-fixed in 2% PFA/1.25% glutaraldehyde overnight at 4°C. The brains were then cryoprotected in 30% (w/v) sucrose (Sigma) in PBS and sectioned coronally at 500 μm on a sliding microtome (Leica). Sections containing the mPFC were then further cut by hand approximately along the dashed lines represented in Figure S1k, and sent to the University of California, San Francisco Pathology Electron Microscopy Core facility for further processing and transmission electron microscopy imaging. Briefly, tissue was post-fixed in 2% osmium tetroxide in 0.1M sodium cacodylate buffer, stained with 2% aqueous uranyl acetate, dehydrated in ethanol, cleared in propyline oxide, and embedded in Eponate 12 (Ted Pella Co). Ultra-thin sections were then collected, beginning from the medial margin, to sample the superficial cortical layers. The sections were subsequently stained with uranyl acetate and Reynold's lead and examined using a Tecnai 10 transmission electron microscope (Philips). The presence of myelinated axons is highly variable in gray matter, and so in order to emphasize the regions of the mPFC with substantial myelin content, we subsampled the three fields of view, per animal, with the highest density of myelinated axons.

Fiber photometry analysis

Freezing behavior during fiber photometry experiments was scored manually in a blinded manner via The Observer (Noldus) as automated scoring was incompatible with movement of the patch cord. Photometry signals were manually aligned to freezing behavior via a light pulse that was output by FreezeFrame and detected by an internally aligned video recording. ΔF/F was calculated by subtracting the linear fit of the isobestic signal to the raw GCaMP signal from the raw GCaMP signal, and then dividing the subsequent result by the linear fit of the isobestic signal to the raw GCaMP signal; i.e., $(465_{raw} - 405_{fitted}) / (405_{fitted})$. Z-scored ΔF/F values were then computed using the mean and standard deviation of the entire recording session. Peri-event analysis was centered on the transitions from bouts of mobility to bouts of freezing that each lasted at least two seconds. The ΔF/F values were extracted from two seconds pre- and post-transition (referred to as pre and post) and the pre mean and post mean are the mean z-scored ΔF/F values within the two seconds pre- and post-bout transition. Peri-event analysis for shock responses were computed similarly, comparing the mean ΔF/F within the five seconds pre- and post-shock.

Histological quantification

All images were acquired with a CSU-W1 spinning disk confocal microscope (Nikon Imaging Center, UCSF. For the basolateral amygdala (BLA) and dorsal hippocampus (dHPC), the entire structure, per hemisection, was quantified as one field. Two fields were quantified manually per section using the multipoint tool in ImageJ, using two to three averaged sections per mouse. Absolute cell counts were normalized to the quantified area and reported as cellular density (cells/mm^2). Myelin basic protein (MBP) fluorescence intensity was quantified by averaging the mean gray value from the Measure function in FIJI[51]. from three non-overlapping fields per brain region per section, with two to three averaged sections per mouse. All comparisons of MBP fluorescence intensity were conducted on sections stained and imaged within the same

sessions, with identical exposure settings used during acquisition. For quantification of GFP^+/MBP^+ myelinating OLs, either cell bodies or non-overlapping GFP^+/MBP^+ arbors were counted as individual cells, with occasional ambiguous cases conservatively quantified as a single cell. All image quantifications were conducted in a blinded manner.

Statistical analysis

No statistical methods were used to predetermine sample size *a priori*, but the sample sizes used are similar to those used in previous studies[15,17]. Two-way ANOVA was used to probe for significant interactions of genotype with freezing behavior across contextual fear conditioning experiments, with Sidak's *post hoc* tests to make single comparisons between genotypes at specific time points. Single comparisons of histological quantifications and fiber photometry parameters were performed via a two-tailed student's *t*-test; paired two-tailed *t*-tests were used for within animal comparisons and unpaired *t*-tests were used for comparisons between genotypes or treatment conditions. Comparisons of histological quantifications or freezing behavior between three or more groups or time points were performed with one-way ANOVA with Sidak's *post hoc* tests. Prism 6 (GraphPad) and MATLAB (Mathworks) were used for all statistical analyses. Data distribution was assumed to be normal but this was not formally tested. For all dot plots and differences reporting, data are presented as mean ± SEM. For all box-and-whisker plots, the center represents the median, the boxes represent the interquartile range, and the whiskers represent the 10^{th} and 90^{th} percentile. Sample sizes and statistical tests used are indicated in the figure legends, with symbols indicating the following p-value ranges: n.s. (not significant) > 0.05, * ≤ 0.05, ** ≤ 0.01, *** ≤ 0.001, **** ≤ 0.0001.

References

1. Hill, R., Patel, K., Goncalves, C., Grutzendler, J., Nishiyama, A. Modulation of oligodendrocyte generation during a critical temporal window after NG2 cell division. *Nat Neurosci* **17,** 1518-1527 (2014).

2. Hill, R., Li, A.M., Grutzendler, J. Lifelong cortical myelin plasticity and age-related degeneration in the live mammalian brain. *Nat Neurosci* **21,** 683–695 (2018).

3. Hughes, E., Kang, S., Fukaya, M., Bergles, D. Oligodendrocyte progenitors balance growth with self-repulsion to achieve homeostasis in the adult brain. *Nat Neurosci* **16,** 668-676 (2013).

4. Hughes, E., Orthmann-Murphy, J., Langseth, A., Bergles, D. Myelin remodeling through experience-dependent oligodendrogenesis in the adult somatosensory cortex. *Nat Neurosci* **21,** 696-706 (2018).

5. Kang, S.H., Fukaya, M., Yang, J.K., Rothstein, J.D., Bergles, D.E. NG2+ CNS glial progenitors remain committed to the oligodendrocyte lineage in postnatal life and following neurodegeneration. *Neuron* **68,** 668-681 (2010).

6. Young, K., et al. Oligodendrocyte dynamics in the healthy adult CNS: evidence for myelin remodeling. *Neuron* **77,** 873-885 (2013).

7. Bergles, D.E., Roberts, J.D., Somogyi, P., Jahr, C.E. Glutamatergic synapses on oligodendrocyte precursor cells in the hippocampus. *Nature* **405**, 187–91 (2000).

8. Lin, S., Bergles, D. Synaptic signaling between GABAergic interneurons and oligodendrocyte precursor cells in the hippocampus. *Nat Neurosci* **7,** 24-32 (2004).

9. Gibson, E., et al. Neuronal activity promotes oligodendrogenesis and adaptive myelination in the mammalian brain. *Science* **344,** 1252304 (2014).

10. Mitew, S., et al. Pharmacogenetic stimulation of neuronal activity increases myelination in an axon-specific manner. *Nat Commun* **9,** 306 (2018).

11. Geraghty, A., et al. Loss of Adaptive Myelination Contributes to Methotrexate Chemotherapy-Related Cognitive Impairment. *Neuron* **103,** 250-265 (2019).

12. Etxeberria, A., et al. Dynamic Modulation of Myelination in Response to Visual Stimuli Alters Optic Nerve Conduction Velocity. *J Neurosci* **36,** 6937–48 (2016).

13. Makinodan, M., Rosen, K.M., Ito, S., Corfas, G. A critical period for social experience-dependent oligodendrocyte maturation and myelination. *Science* **337,** 1357-1360 (2012).

14. Mangin, J.M., Li, P., Scafidi, J., Gallo, V. Experience-dependent regulation of NG2 progenitors in the developing barrel cortex. *Nat Neurosci* **15,** 1192-1194 (2012).

15. McKenzie, I.A., et al. Motor skill learning requires active central myelination. *Science* **346,** 318-322 (2014).

16. Liu, J., et al. Impaired adult myelination in the prefrontal cortex of socially isolated mice. *Nat Neurosci* **36,** 957-962 (2012).

17. Xiao, L., et al. Rapid production of new oligodendrocytes is required in the earliest stages of motor-skill learning. *Nat Neurosci* **19,** 1210-1217.

18. Tripathi, R.B., et al. Remarkable Stability of Myelinating Oligodendrocytes in Mice. *Cell Reports* **21,** 316-323 (2017).

19. Pan, S., Chan, J.R. Regulation and dysregulation of axon infrastructure by myelinating glia. *J Cell Bio* **216,** 3903-3916 (2017).

20. de Hoz, L., Simons, M. The emerging functions of oligodendrocytes in regulating neuronal network behaviour. *BioEssays* **37,** 60–69 (2015).

21. Shalev, A., Liberzon, I., Marmar, C. Post-Traumatic Stress Disorder. *N Engl J Med* **376,** 2459-2469 (2017).

22. Tovote, P., Fadok, J.P., Lüthi, A. Neuronal circuits for fear and anxiety. *Nat Rev Neurosci* **16,** 317-331 (2015).

23. Cowansage, K.K., et al. Direct reactivation of a coherent neocortical memory of context. *Neuron* **84,** 432–41 (2014).

24. DeNardo, L.A., et al. Temporal evolution of cortical ensembles promoting remote memory retrieval. *Nat Neurosc*i **22,** 460 (2019).

25. Kitamura, T., et al. Engrams and circuits crucial for systems consolidation of a memory. *Science* **356,** 73-78 (2017).

26. Tanaka, K.Z. Cortical representations are reinstated by the hippocampus during memory retrieval. *Neuron* **84,** 347-354 (2014).

27. Vetere, G., et al. Chemogenetic Interrogation of a Brain-wide Fear Memory Network in Mice. *Neuron* **94,** 363-374 (2017).

28. Frankland, P.W., Bontempi, B. The organization of recent and remote memories. *Nat Rev Neurosci* **6,** 119 (2005).

29. Tonegawa, S., Morrissey, M., Kitamura, T. The role of engram cells in the systems consolidation of memory. *Nat Rev Neurosci* **19,** 485-498 (2018).

30. Emery, B., et al. Myelin Gene Regulatory Factor Is a Critical Transcriptional Regulator Required for CNS Myelination. *Cell* **138,** 172–185 (2009).

31. Giustino, T.F., Fitzgerald, P.J., Maren, S. Fear Expression Suppresses Medial Prefrontal Cortical Firing in Rats. *PLoS ONE* **11,** e0165256 (2016).

32. Halladay, L.R., Blair, H.T. Distinct ensembles of medial prefrontal cortex neurons are activated by threatening stimuli that elicit excitation vs. inhibition of movement. *J. Neurophysiol.* **114,** 793–807 (2015).

33. Mei, F., et al. Micropillar arrays as a high-throughput screening platform for therapeutics in multiple sclerosis. *Nat Med* **20,** 954-960 (2014).

34. Mei, F., et al. Accelerated remyelination during inflammatory demyelination prevents axonal loss and improves functional recovery. *Elife* **5,** pii: e18246 (2016).

35. Green, AJ, Gelfand, JM, Cree, BA, Lancet, B.-C. Clemastine fumarate as a remyelinating therapy for multiple sclerosis (ReBUILD): a randomised, controlled, double-blind, crossover trial. *The Lancet* **390,** 2481-2489 (2017).

36. Liu, J., et al. Clemastine Enhances Myelination in the Prefrontal Cortex and Rescues Behavioral Changes in Socially Isolated Mice. *J Neurosci* **36,** 957–962 (2016).

37. Wang, F.,et al. Enhancing Oligodendrocyte Myelination Rescues Synaptic Loss and Improves Functional Recovery after Chronic Hypoxia. *Neuron* **99,** 689-701 (2018).

38. Guo, N., et al. Dentate granule cell recruitment of feedforward inhibition governs engram maintenance and remote memory generalization. *Nat Med* **24,** 438-449 (2018).

39. Freeman, S.A., et al. Acceleration of conduction velocity linked to clustering of nodal components precedes myelination. *Proc. Natl. Acad. Sci. U.S.A.* **112,** 321–8 (2015).

40. Fünfschilling, U., et al. Glycolytic oligodendrocytes maintain myelin and long-term axonal integrity. *Nature* **485,** 517-522 (2012).

41. Lee, Y., et al. Oligodendroglia metabolically support axons and contribute to neurodegeneration. *Nature* **487**, 443-448 (2012).

42. Xin, W., et al. Oligodendrocytes Support Neuronal Glutamatergic Transmission via Expression of Glutamine Synthetase. *Cell Rep* **27,** 2262–2271 (2019).

43. Frankland, P.W., Bontempi, B., Talton, L.E., Kaczmarek, L., Silva, A.J. The involvement of the anterior cingulate cortex in remote contextual fear memory. *Science* **304,** 881–3 (2004).

44. Maviel, T., Durkin, T., Menzaghi, F., Bontempi, B. Sites of Neocortical Reorganization Critical for Remote Spatial Memory. *Science* **305,** 96-99 (2004).

45. Benchenane, K., et al. Coherent Theta Oscillations and Reorganization of Spike Timing in the Hippocampal- Prefrontal Network upon Learning. *Neuron* **66,** 921–936 (2010).

46. Karalis, N., et al. 4-Hz oscillations synchronize prefrontal-amygdala circuits during fear behavior. *Nat Neurosci* **19,** 605-612 (2016).

47. Xia, F., et al. Parvalbumin-positive interneurons mediate neocortical-hippocampal interactions that are necessary for memory consolidation. *Elife* **6,** pii: e27868 (2017).

48. Pajevic, Basser, P.J., Fields, R.D. Role of myelin plasticity in oscillations and synchrony of neuronal activity. *Neuroscience* **276,** 135-147 (2014).

49. Steadman, P.E., et al. Disruption of Oligodendrogenesis Impairs Memory Consolidation in Adult Mice. *Neuron*, https://doi.org/10.1016/j.neuron.2019.10.013 (2019).

50. Chao, L., Tosun, D., Woodward, S., Kaufer, D., Neylan, T.. Preliminary Evidence of Increased Hippocampal Myelin Content in Veterans with Posttraumatic Stress Disorder. *Front Behav Neurosci* **9,** 333 (2015).

51. Chen T.W., et al. Ultrasensitive fluorescent proteins for imaging neuronal activity. *Nature* **499,** 295-300 (2013).

52. Schindelin, J., et al. Fiji: an open-source platform for biological-image analysis. *Nat Methods* **9,** 676-682 (2012).

Publishing Agreement

It is the policy of the University to encourage open access and broad distribution of all theses, dissertations, and manuscripts. The Graduate Division will facilitate the distribution of UCSF theses, dissertations, and manuscripts to the UCSF Library for open access and distribution. UCSF will make such theses, dissertations, and manuscripts accessible to the public and will take reasonable steps to preserve these works in perpetuity.

I hereby grant the non-exclusive, perpetual right to The Regents of the University of California to reproduce, publicly display, distribute, preserve, and publish copies of my thesis, dissertation, or manuscript in any form or media, now existing or later derived, including access online for teaching, research, and public service purposes.

DocuSigned by:
Simon Pan
DCBB254418EF46D...
Author Signature

3/16/2020
Date